Development of Impurity Profile Diagnostics in the Ergodic Layer of LHD using 3 m Normal Incidence VUV Spectrometer*)

Tetsutarou OISHI, Shigeru MORITA, Chunfeng DONG, Erhui WANG[1)],
Motoshi GOTO and LHD Experiment Group

National Institute for Fusion Science, 322-6 Oroshi-cho, Toki 509-5292, Japan
[1)]*Department of Fusion Science, Graduate University for Advanced Studies, 322-6 Oroshi-cho, Toki 509-5292, Japan*

(Received 26 November 2012 / Accepted 23 April 2013)

Space-resolved vacuum ultraviolet (VUV) spectroscopy using a 3 m normal incidence spectrometer has been developed in the large helical device (LHD) to study plasma transport in the ergodic layer by measuring the spatial profile of VUV lines from impurities emitted in the wavelength range of 300-3200 Å. Characteristics of the diagnostics system such as line dispersion, observable region and spatial resolution were evaluated. CIV spectra of 1548.20×2 Å were measured clearly. Intensity and ion temperature profiles were obtained simultaneously using CIV emissions in high-density discharges. Dependencies of the CIV intensity profiles on the electron density and magnetic configurations were observed.

Keywords: VUV spectroscopy, impurity transport, normal incidence spectrometer, space-resolved diagnostics, large helical device, ergodic layer, stochastic magnetic field, carbon ion, ion temperature measurement

DOI: 10.1585/pfr.8.2402093

1. Introduction

Control of the impurity transport in the edge region of magnetically-confined plasmas has attracted attention in fusion research for sustaining high-performance plasma and mitigation of the divertor heat flux. For this purpose, edge impurity transport and its effect on plasma performance have been investigated in tokamak and helical devices [1, 2]. In particular, impurity studies on the edge stochastic magnetic field layer have recently been attracted. For example, reduction of the cross-field impurity transport, so called "impurity screening", was observed in the large helical device (LHD), which is a large-sized superconducting heliotron device having a major radius of 3.6 m, averaged minor radius of 0.64 m, toroidal magnetic field of 3 T, toroidal period number of 10 and poloidal mode number of 2 [3]. The impurity screening phenomenon is due to the presence of a thick stochastic magnetic field layer called "ergodic layer", located outside the core plasma. Measurement of emissions from impurity carbon ions in a variety of ionization stages has clarified that the impurity screening depends on the thickness of the ergodic layer [4]. A precise measurement of the spatial profile of impurity line emissions in the ergodic layer is required to investigate such effects of the ergodic layer in detail.

The thickness of the ergodic layer surrounding the last closed flux surface (LCFS) ranges from several to several tens of centimeters, and has poloidal and toroidal variations, while it depends on the position of the magnetic axis. Vacuum ultraviolet (VUV) lines from impurity ions are significantly emitted in the ergodic layer because the electron temperature around LCFS ranges from 10 to 500 eV [5]. Space-resolved spectroscopy has been applied to measure the intensity profiles of the line emission from the impurities in the ergodic layer. A 3 m normal incidence spectrometer has favorable characteristics for measuring VUV emissions in the wavelength range of 300-3200 Å [6, 7]. In this paper, details of a diagnostic system for impurity profile measurement in the ergodic layer of LHD are presented with preliminary experimental results.

2. Development of Diagnostics Systems

Figure 1 shows a schematic drawing of the diagnostics system. A 3 m normal incidence VUV spectrometer (McPherson model 2253) was installed on a horizontal diagnostic port (#10-O). This spectrometer has been used for observation of intrinsic impurity lines [8] and identification of forbidden magnetic dipole emission lines [9–11] in LHD. In this study, the optical axis was arranged perpendicular to the toroidal magnetic field in the bottom edge at a horizontally-elongated plasma cross section to adjust the observable region to the ergodic layer. The wavelength resolution is 0.15 Å when the entrance slit is set to 20 μm in width and a 1200 g/mm grating is used. A back-illuminated CCD detector (Andor model 435: 1024×1024 ch) is placed at the position of the exit

author's e-mail: oishi@LHD.nifs.ac.jp
*) This article is based on the presentation at the 22nd International Toki Conference (ITC22).

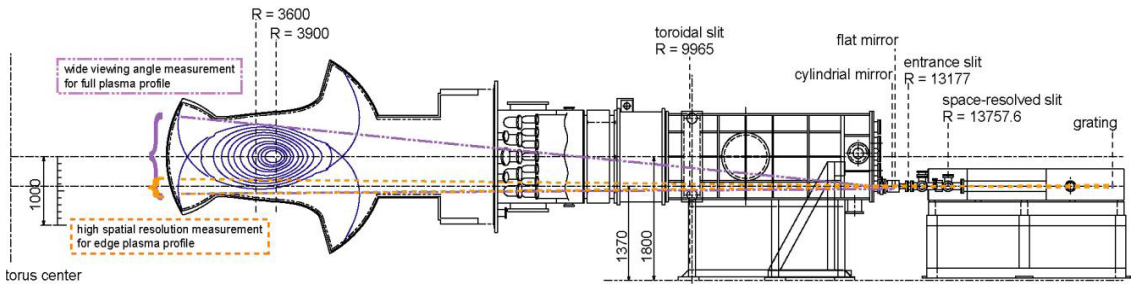

Fig. 1 Poloidal cross section of LHD and impurity diagnostics system for study of ergodic layer using space-resolved 3 m VUV spectrometer.

slit. The size of the CCD is $13.3 \times 13.3\,\mathrm{mm}^2$, and the pixel size is $13 \times 13\,\mu\mathrm{m}^2$. The wavelength dependence of the line dispersion of the spectrometer was evaluated using well-known spectral lines of CIV (1548.20 Å, 1550.77 Å and their second order), Lyman α (1215.67×2 Å), CIII (574.281 Å), HeI (584.334 Å), and OIII (599.59 Å). It changed almost linearly from 0.0362 to 0.0370 Å/pix, while the wavelength changes from 300 to 3200 Å. Then, the wavelength interval which can be measured in a single discharge is about 37 Å.

The vertical profile of VUV emissions as a wavelength-dispersed image is projected on the CCD detector by a slit designed for spatial resolution called the "space-resolved slit" mounted between the entrance slit and the grating in the spectrometer. The vertical width of the space-resolved slit can be controlled from 50 to 14000 μm, and it determines the spatial resolution. We applied the evaluation method of the spatial resolution by measuring the profiles of CIV 1548.20×2 Å emission intensity with scanning width of the slit [12]. It is known that the spatial profile of the CIV intensity has a steep peak in the ergodic layer [13–16]. As a result of scanning the slit width, the intensity increased with the slit width, while the peak position of the intensity changed inwardly and the width of the peaked profile became broader when an extremely wider slit was used. This indicates the degradation of the spatial resolution based on the distortion of measured profiles. A slit width of around 500 μm was thus appropriate for compatibility of the intensity and the spatial resolution.

A mirror unit consisting of a flat mirror and a cylindrical mirror was designed and installed between the spectrometer and the torus to switch the view angle, as shown in Fig. 1. The sightline is basically adjusted to measure the edge plasma profile with high-spatial resolution, while it can be expanded to measure the full plasma profile with a wider viewing angle if the mirror unit is used. To limit the observable region in the toroidal direction, a rectangular aperture called the "toroidal aperture" is mounted in the housing of the mirror unit. For the edge profile measurement, the toroidal aperture width can be selected from among 0.4, 1.0, and 2.0 mm, corresponding to the toroidal intervals in the observable region of 19.5, 48.8,

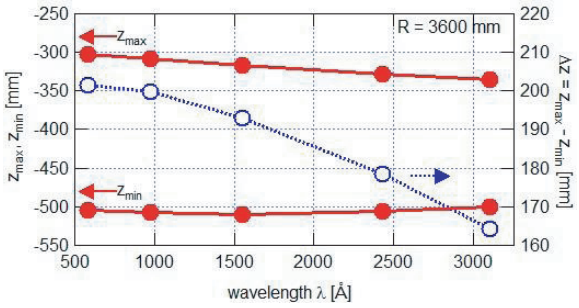

Fig. 2 Wavelength dependence of the observable region for edge profile measurement. Maximum position z_{max} and minimum position z_{min}, and vertical range of the observable region $z = z_{max} - z_{min}$ at $R = 3600$ mm are shown together.

and 97.6 mm at the major radius $R = 3600$ mm, respectively. For the full profile measurement, a toroidal aperture of 1.6 mm is used and corresponds to 98.9 mm toroidal interval of the observable region at $R = 3600$ mm.

Precise calibration of the observable region for different wavelengths is required because the distance between the grating and the entrance slit automatically changes with the wavelength to be adjusted to the wavelength-dependent focal length, which causes a change of view angle against the wavelength. To determine the vertical position of the observable region absolutely, a toroidally-movable slit with a rectangular-corrugated edge located at $R = 9965$ mm is utilized [13]. The vertical width with opened space of the rectangular corrugated edge changes monotonically in the vertical direction. Therefore, we can determine the vertical position of the observable region by measuring the image of line emissions from LHD plasmas through the rectangular-corrugated slits. This calibration was applied to both cases in the edge profile measurement without the mirror unit and the full profile measurement with the mirror unit. Figure 2 shows the dependence of the observable region for the edge profile measurement on the wavelength. The maximum position z_{max} and minimum position z_{min}, and the vertical range of the observable region $\Delta z = z_{max} - z_{min}$ at $R = 3600$ mm are shown together. CIV (1548.20 Å and its second order), Lyman α (1215.67×2 Å), CIII (977.020 Å), and ArVII (585.750 Å)

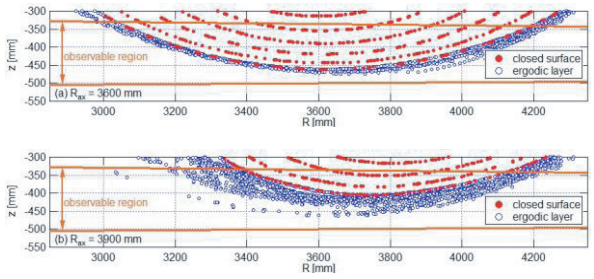

Fig. 3 Enlarged view of the observable region for the wavelength of 3105 Å on the Poincare plot of vacuum magnetic fields with the magnetic axis R_{ax} = (a) 3600 and (b) 3900 mm.

are used to evaluate the wavelength dependence of the observable region. Figure 3 shows the enlarged view of the observable region on the Poincare plot of the vacuum magnetic fields with the magnetic axis of R_{ax} = 3600 and 3900 mm. The observable region was evaluated for the wavelength of 3105 Å, which is adjusted to measure the CIV line of 1548.20 × 2 Å. In the R_{ax} = 3900 mm configuration, the ergodic layer is wider and the position of LCFS becomes more internal than in R_{ax} = 3600 mm at the bottom edge [17]. The observable region can cover the whole range of the ergodic layer at the bottom edge in both cases of the magnetic axis.

3. Results of Measurements

Preliminary VUV spectroscopy data were measured in high-density discharges of LHD using the system developed in the present study. Hydrogen plasma was initiated by electron cyclotron heating and further heated by neutral beams with negative ion sources (NBI #1, 2, 3). In this section, results obtained using sightlines with high spatial resolution measurement for the edge plasma profile are reported. Note that the z-coordinate of sightlines at R = 3600 mm evaluated with the wavelength of 3105 Å is used for the horizontal axis of the measured spatial profiles. Conditions of the diagnostics are as follows: time resolution of 100 milliseconds, entrance slit width of 20 μm, space-resolved slit width of 600 μm, toroidal aperture width of 1.0 mm, number of sightlines of 51 ch (20 pixels binning is applied for 1 ch), and grating blaze wavelength of 3105 Å.

Figure 4 (a) shows a wavelength spectrum in the full wavelength range covered in a single discharge including CIV lines with wavelengths of 1548.20 × 2 and 1550.77 × 2 Å. The line shape of the wavelength spectrum $I(\lambda)$ has a Gaussian profile if it is assumed that the ions have a Maxwellian velocity distribution as follows:

$$I(\lambda)\frac{1}{\sqrt{\pi}\Delta_D}\exp\left(-\frac{(\lambda-\lambda_0)^2}{{\Delta_D}^2}\right), \quad (1)$$

where λ_0 is the center wavelength and Δ_D is the Doppler width. The Doppler width at full width at half maximum

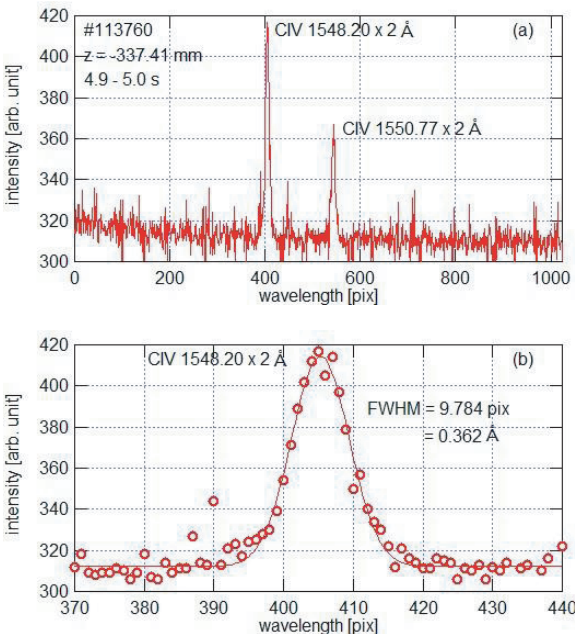

Fig. 4 Wavelength spectrum of CIV lines in (a) the full wavelength range covered in a single discharge and (b) the enlarged view around the peak of 1548.20 × 2 Å together with the fitted Gaussian function.

(FWHM), Δ_{FWHM}, is given by $\Delta_{FWHM} = 2\,(\ln 2)^{1/2}\,\Delta_D$. The ion temperature T_i in eV is thus given by $T_i = 1.68 \times 10^8\, M\,(\Delta_{FWHM}/\lambda_0)^2$, where M is the atomic mass number. Figure 4 (b) is the enlarged view of the measured CIV spectrum around the peak of 1548.20 × 2 Å together with the Gaussian profile as a fitting function. It is reasonable that we assume a single T_i because the experimental data can be fitted well by a single Gaussian profile. The FWHM of the fitted profile is 0.362 Å in this figure. Deconvoluting the instrumental function of 0.15 Å in FWHM measured using a mercury lamp from the FWHM of the fitted profile, Δ_{FWHM} = 0.359 Å and T_i = 27.1 eV are obtained. The accuracy of T_i is determined by the fitting error of the Doppler width of the Gaussian profile. It corresponds to the error of the ion temperature $\Delta T_i = \pm 1.6$ eV for the profile shown in Fig. 4 (b).

Figure 5 shows the vertical profiles of the CIV line intensity and T_i obtained in the discharges at R_{ax} = 3600 mm with different electron densities. The LCFS of the vacuum magnetic field is indicated with an arrow. The data from about $z = -380$ to -390 mm are missing in the following spatial profiles because a metal wire installed in the optics for the alignment of the sightlines is projected onto the corresponding position of the CCD. The line-averaged electron density was scanned from 4 to $8 \times 10^{19}\mathrm{m}^{-3}$ by controlling the amount of gas puffing. The peaked structure in the edge intensity profile became clearer in higher electron density discharges. It has been recognized that the CIV emission is released only in the outermost region of the ergodic layer in LHD plasmas because the low ion-

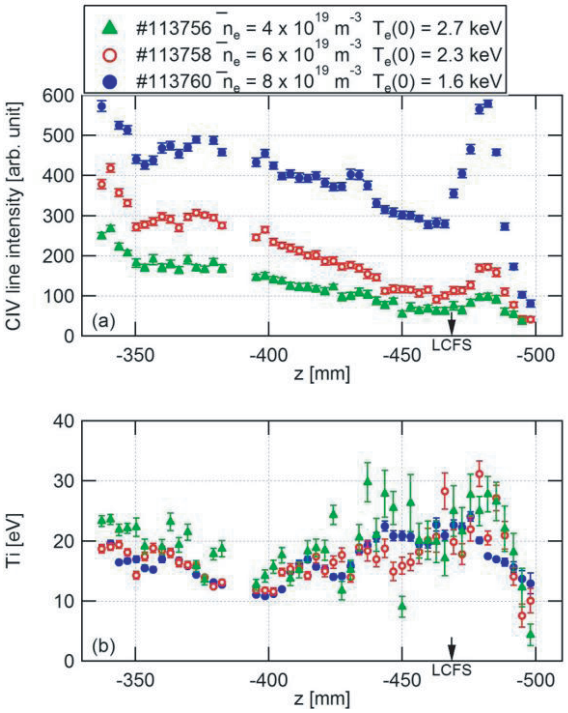

Fig. 5 Vertical profiles of (a) CIV line intensity and (b) ion temperature derived from the Doppler broadening of CIV spectrum. Profiles at different electron densities are shown together.

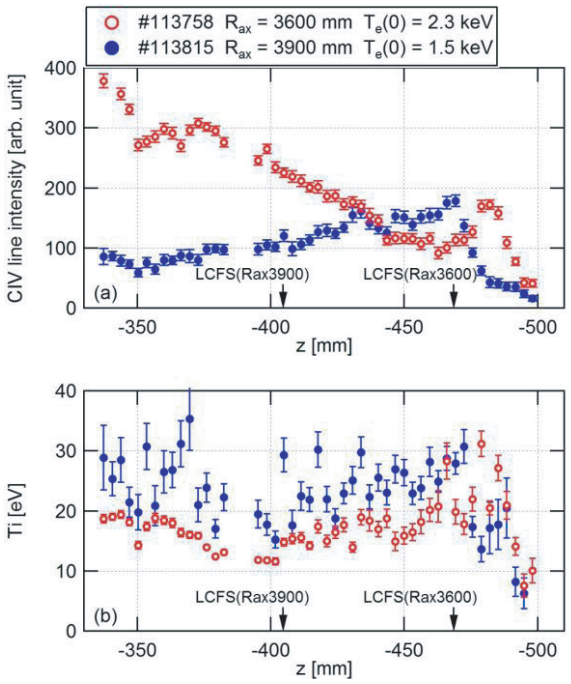

Fig. 6 Vertical profiles of (a) CIV line intensity and (b) ion temperature derived from the Doppler broadening of CIV spectrum. Profiles for different magnetic axes are shown together.

ization energy of 65 eV for C^{3+} ions causes less fractional abundance in the core plasma. Therefore, the peak of the intensity profile outside LCFS shown in Fig. 5 is a result of line integration in a long path along the sightline through the ergodic layer at the bottom edge of the horizontally-elongated elliptical plasma. In addition, the intensity starts to increase again as the position of the sightline moves upward from LCFS. This is because the length of the line integral path along the sightline through the ergodic layer becomes longer in the observable region closer to the midplane. The T_i profile also indicates the edge T_i in the ergodic layer at corresponding vertical positions. The amplitudes of the error bars in the T_i measurement depend on the signal intensities because the fitting error of the Gaussian profile increases in cases with less signal intensity. It has not been clarified at present whether or not the T_i profile has a density-dependent spatial structure.

Figure 6 shows the profiles of CIV line intensity and T_i for R_{ax} = 3600 and 3900 mm. The line-averaged electron density is 6×10^{19} m^{-3} for both shots. The edge intensity profile of CIV in R_{ax} = 3900 mm shows a peak at the inner position and a broader distribution compared to the result from R_{ax} = 3600 mm. This result is consistent with the fact that the thickness of the ergodic layer becomes wider in R_{ax} = 3900 mm and the LCFS shifts inward at the bottom edge of the plasma as shown in Fig. 3. The value of T_i seems to be slightly higher in R_{ax} = 3900 mm compared with that in R_{ax} = 3600 mm. The physical interpretation of this difference remains as a future study.

4. Summary

Space-resolved VUV spectroscopy using a 3 m normal incidence spectrometer was developed in LHD to study the plasma transport in the ergodic layer. The spatial profile of VUV lines from impurities was measured in the wavelength range of 300 - 3200 Å. The optical axis of the spectroscopic system was arranged perpendicular to the toroidal magnetic field at the bottom edge of a horizontally-elongated plasma cross section to adjust the observable region to the ergodic layer. The observable region was calibrated precisely for different wavelengths to be adjusted to the wavelength-dependent focal length. As preliminary results, intensity and ion temperature profiles were obtained simultaneously using the CIV spectra of 1548.20 × 2 Å in high-density discharges. The intensity profile showed a peak structure outside LCFS as a result of line integration in a long path along the sightline through the ergodic layer. The position and width of the peak structure varied depending on the position of LCFS and the thickness of the ergodic layer, respectively. This system will be utilized in impurity studies such as line identification or particle transport to investigate the edge plasma physics, especially on the role of the ergodic layer.

Acknowledgment

This work was partly supported by the JSPS-NRF-NSFC A3 Foresight Program in the field of Plasma Physics (NSFC: No.11261140328).

[1] P.C. Stangeby and G.M. McCracken, Nucl. Fusion **30**, 1225 (1990).
[2] R. Burhenn *et al.*, Nucl. Fusion **49**, 065005 (2009).
[3] M. Kobayashi *et al.*, Proc. 22nd Int. Conf. on Fusion Energy, Geneva, Switzerland, 13-18 October 2008 (Vienna: IAEA), EX/9-4 "Study on impurity screening in stochastic magnetic boundary of the Large Helical Device" (2008).
[4] M.B. Chowdhuri *et al.*, Phys. Plasmas **16**, 062502 (2009).
[5] S. Morita *et al.*, Plasma Phys. Control. Fusion **48**, A269 (2006).
[6] S. Morita and M. Goto, Rev. Sci. Instrum. **74**, 2036 (2003).
[7] R. Katai *et al.*, Rev. Sci. Instrum. **77**, 10F307 (2006).
[8] R. Katai *et al.*, Plasma Fusion Res. **2**, 014 (2007).
[9] R. Katai *et al.*, J. Plasma Fusion Res. SERIES **7**, 9 (2006).
[10] R. Katai *et al.*, J. Quant. Spectrosc. Radiat. Transfer **107**, 120 (2007).
[11] S. Morita *et al.*, Plasma Sci. Technol. **12**, 341 (2010).
[12] C.F. Dong *et al.*, Rev. Sci. Instrum. **81**, 033107 (2010).
[13] C.F. Dong *et al.*, Phys. Plasmas **18**, 082511 (2011).
[14] C.F. Dong *et al.*, Plasma Fusion Res. **6**, 2402078 (2011).
[15] C.F. Dong *et al.*, Plasma Sci. Technol. **13**, 140 (2011).
[16] E.H. Wang *et al.*, Plasma Fusion Res. **7**, 2402059 (2012).
[17] T. Morisaki *et al.*, J. Nucl. Mater. **313-316**, 548 (2003).